JOURNAL OF Materials CHEMISTRY

Investigation of contact interactions of (001) MgO: molecular dynamics simulations studies

C. W. Yong,*[a] W. Smith[a] and K. Kendall[b]

[a]*CCLRC, Daresbury Laboratory, Daresbury, Warrington, UK WA4 4AD. E-mail: c.w.yong@dl.ac.uk*
[b]*School of Chemical Engineering, The University of Birmingham, Edgbaston, Birmingham, UK B15 2TT*

Received 27th June 2001, Accepted 14th November 2001
First published as an Advance Article on the web 23th January 2002

Molecular dynamics simulations have been performed to investigate surface contact interactions between small MgO probes (blocks of cross-section $n \times n$ atoms, where $n = 2$, 4, 6, 8 and 10), and the MgO (001) surface (periodic MgO slabs) at 300 K. The contact behaviour was monitored by measuring the force on the probe and the interplanar spacings at different vertical distances between the probe and slab. A mechanistic description of the probe's approach has thus been obtained. In all cases, a characteristic instability 'jump' was observed, where the probe was attracted towards the surface, signalled by large atomic displacements and an increased attractive force. It was found that the normal force per atom experienced by a probe decreases as the area increases and could be characterised by a logarithmic exponent, $q = 0.12$ (corresponding simulations for NaCl have yielded a similar value). Hysteresis occurred in every case after the jump and a rich variety of phenomena were observed, such as 'neck' formation, accompanied by atomic dislocations, and systematic removal of atoms from the surface, as the probe was withdrawn.

Introduction

Granular materials such as sand and powders exhibit a great variety of complex behaviours that are neither completely solid-like nor fluid-like[1] For example, the excitation and flow studies of these materials show complex patterns similar to those of ordinary liquids. However, they can also resist shear and undergo hysteresis and plastic deformation. This dual-nature behaviour indicates that granular materials cannot be adequately described by simple bulk equations of motions such as the usual hydrodynamic equations.[2]

One of the main factors that distinguish granular materials from molecular systems is that contact interactions in the former case are inelastic in nature. In other words, energy is lost on particle contact (principally as heat) and in the absence of a replenishing energy source, the particles lose kinetic energy, such that the whole system eventually comes to a complete halt. In computer simulations, inelastic collisions are often modelled by introducing some frictional damping forces at the point of contact.[3] In some cases, static friction is also introduced to mimic the static behaviour of granular material.[3,4] Using such simple models, many interesting granular phenomena, such as heap formation[5] and inelastic collapse,[6] have been reproduced. However, most of the simulations to date have used featureless rigid disks or spheres as model particles, each assigned a single frictional parameter. Such an approach is not based on any sound scientific justification. In a real granular material, contact interactions between particles are very complicated and thus difficult to characterise. This is due to the large variation in size and surface roughness among the granular particles. Thus more sophisticated models have been devised by introducing some effective contact parameters which depend on the size, shape and distance variation between two neighbouring particles.[7,8] However, the models ignore hysteresis during tangential contacts. In reality, exchange of particle components may occur during contact, which has the potential to alter the frictional behaviour between individual particles. Furthermore, other simulation studies have managed to give better agreement with the experimental results by simulating non-spherical particles without an explicit expression for static friction.[9] Clearly, this indicates that studies of contact forces are both important and incompletely understood, despite much work dedicated to this area of study.[10]

Friction occurs whenever two moving bodies come into contact. As the bodies slide against each other an opposing frictional force arises which acts parallel but opposite to the sliding direction. There may be several intertwining factors that contribute to the overall observed phenomenon. For example, it may be attributed to the atomistic interaction between the constituent atoms of contacting bodies. Friction usually leads to surface deformation and wear,[11] which may involve the exchange of atoms between the contact bodies. However, in some cases, two sliding bodies may generate friction without wear, even at the atomistic level.[12] Thus, friction can be manifested in a rich variety of ways and identifying key common factors to characterise friction is obviously highly desirable.

It is possible to investigate friction at an atomistic level. Unfortunately, the coefficient of friction obtained from experiment is usually phenomenologically derived.[13] It does not relate directly to the atomistic origin of friction, nor shed light on the underlying atomistic mechanisms involved. Experimentally, it was only quite recently that surface-sensitive equipment, such as atomic force microscopy, was devised to probe sliding surfaces at atomic resolutions.[14–16] Even then the results are usually complicated by undesirable factors such as surface defects and the presence of contaminants. To this end, theoretical[17–19] and molecular dynamics (MD) computer simulation methods have been pursued to complement experimental studies. A large number of simulation studies have been carried out to investigate the nature of sliding friction between surfaces, with[20,21] or without[22,23] the presence of lubricating atoms. In addition, numerous simulation studies of indentation and sliding of a material tip on a surface have been carried out.[24–26] These studies provide valuable mechanistic views on

This journal is © The Royal Society of Chemistry 2002

friction at the atomic scale. However, there is still a lack of details regarding the underlying factors that contribute to frictional forces.

It is our aim to investigate systematically the atomistic factors underlying friction and to establish links from these to the macroscopically observed frictional phenomena. Obviously, such studies are particularly relevant to the understanding of the contact mechanics of granular materials. Due to the complexity of the subject, we cannot wholly quantify friction at this stage. Rather, in this paper, we report our investigation on the effects of contact between two bodies in atomistic detail. Although surface roughness is a very important parameter in determining frictional force, the first requirement for friction to occur is for two bodies to make contact with each other. In fact, there have been a few other computer simulation studies of surface contact done in the past, such as the adhesion and compression of diamond surfaces.[27] In this paper we have considered simple, commensurate contact between two (001) magnesium oxide (MgO) surfaces and we have used MD simulations in order to study the nature of the contacts. MgO is commonly used as a model system for understanding interfacial processes on metal oxides. Furthermore, MgO can readily produce well-defined nanometer-size particulate material, suitable for experimental study. It is therefore an ideal choice for the purpose of our study.

Methodology

Model

In a real system, the surface is rarely perfectly flat and contact between two macroscopic bodies will occur in a number of discrete areas. For this reason 'surface-to-surface' contact is considered rare. A much more likely occurrence is 'point-to-surface' contact, whereby a raised projection of one body makes contact with the surface of the other. In order to simulate the 'point-to-surface' contact our model system consisted of a slab of the periodic MgO (001) surface and an isolated MgO block of finite cross-sectional area. For simplicity, we refer to these as the slab and the probe respectively. The slab was represented as 16×16 rows of MgO (2.104 Å) lattice 6 layers deep, which gives a total of 1536 atoms. Periodic boundary conditions were applied parallel to the surface so that an infinite crystal surface was produced. A periodicity normal to the surface (z-direction) was introduced so that a vacuum gap existed between two surfaces in the resulting supercell, which was about 39 Å.

Each probe was modelled as a MgO block 6 layers thick. Five probes of different cross-sectional area ($n \times n$ atoms, where $n = 2$, 4, 6, 8 and 10) were constructed, representing different degrees of surface roughness. Initially, a probe was placed at some distance above the slab, where slab–probe interactions were negligible. The probe was arranged to enable commensurate contact between the bulk and probe surfaces at close contact. The size of the slab ensured that there was no interaction between probes of all sizes with their x–y periodic image counterparts. Furthermore, the large vacuum gap ensured that the probe interacted significantly only with the nearest image of the slab in the z-direction. For ease of description, we refer to the surfaces of the probe and slab that are closest (*i.e.* interacting) as the active surfaces, and the most distant (non-interacting) surfaces as base surfaces.

Molecular dynamics

The numerical simulations were performed using the computer package DL_POLY.[28] The purpose of each simulation was to advance the probe towards the slab surface at a rate sufficiently slow to guarantee thermodynamic equilibrium at all times. All atoms from the base surfaces were held in a rigid layer. Atoms situated at the two lattice layers above the base surface were coupled to the Berendsen heat bath[29] maintained at 300 K. These atoms helped to regulate the temperature of the whole system. Atoms from the next three layers, including those from the active surfaces were allowed to move freely without constraint or thermal heat bath. Fig. 1 shows schematically an example model as described above. All atoms were treated as rigid ions interacting *via* pairwise short ranged Buckingham potentials, for which the parameters were obtained from Catlow *et al.*[30] The long range electrostatic potentials were evaluated by means of the Ewald summation, using formal charge values for Mg and O of +2.0 and −2.0 respectively. Care was taken to ensure the Ewald summation for each system was properly converged by comparing the Coulombic energy and its virial counterpart where both are essentially the same magnitude with typical differences of less than 0.1%. Classical Newtonian trajectories were solved by the Verlet leap-frog algorithm[31] with a fixed time-step of 0.5 fs.

All atoms, with the exception of the rigid atoms, were initially assigned a random Gaussian distribution of velocities with an equivalent temperature of 300 K. All systems were allowed to equilibrate for 90 ps, long enough to achieve a stable mean configurational energy. After equilibration, the probe was moved towards the bulk slab with a step of 0.5 Å every 2000 time steps, the change in distance being measured between the rigid bases of the probe and slab. (This is equivalent to a movement of 5 m $^{-1}$s, which is a typical speed encountered in the flow of granular materials.) After each advance, the system was allowed to equilibrate for 1000 time steps (0.5 ps). This was followed by data sampling and averaging over a further 1000 time steps. Note that the base surfaces were held fixed during each equilibration–sampling cycle. Care was taken to ensure that after each increment, the equilibration cycle was sufficiently long for the system to equilibrate before data measurements were recorded. The procedure was repeated many times, so that the probe interaction with the slab surface up to contact and beyond could be obtained.

In a second series of experiments, a similar procedure to that above was adopted to withdraw the probe from the surface.

We have taken the normal distance, d_z (Fig. 1), between the rigid planes of slab and probe as the measure of the probe–surface distance and we have measured the normal force (along the z direction) per atom, F_z, at the rigid plane of the probe. (Note that d_z is not the distance between the active surfaces of the probe and slab.) In addition, the first three interplanar spacings closest to the active surfaces were also measured, to monitor the change in crystal surface structure during the contact process. The three spacings are denoted as P1, P2, P3 for the probe and S1, S2, S3 for the surface (see Fig. 1). Initially, all probes were placed at a distance of $d_z = 28$ Å

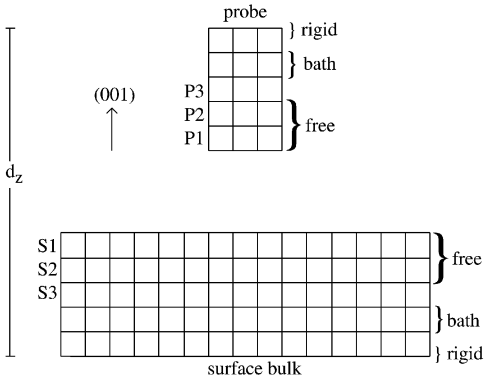

Fig. 1 Schematic representation of the model as described in the text. Refer to the Methodology section for descriptions of the notations.

which left a gap of about 7 Å between the active surfaces of the slab and probe.

Results

Probe approach to the surface

Overview of F_z profiles. Fig. 2 shows the calculated profile of F_z *versus* d_z for different sized probes, as the probe approached the surface. Broadly speaking, the profiles are qualitatively similar for all cases. At the largest values of d_z the average force is approximately zero or slightly negative. A negative value indicates that an attractive force is experienced by the rigid plane of the probe as it moves towards the slab. As d_z diminishes, F_z becomes progressively more negative until at a critical distance, the force 'jumps' to a more negative value, after which it changes in a positive direction until it reaches zero force. With further reduction in d_z, the force F_z becomes positive, indicating a repulsive force. The repulsive force continues to increase as d_z decreases.

Thus we identify four distinct regions of the F_z profiles: (i) a region of weak attraction; (ii) the jump region; (iii) the approach to zero force; and (iv) the repulsion region.

(i) Region of weak attraction. At large d_z, it is apparent that the probe is only weakly attracted by the surface, signifying negligible interaction between the probe and the slab, and that the former is still effectively in an isolated state. The origins of the attraction are the electrostatic and van der Waals forces, the latter of which are just within the applied cutoff range at the largest d_z value. There is no significant change in either the probe or surface structure in this region, which implies that withdrawal of the probe at this stage would occur without complications.

(ii) The jump region. The most interesting feature in Fig. 2 is the significant change in F_z, which occurs over a very short distance, though at different locations for different probes. It appears that the location (d_z^{jump}) and magnitude of the jump is a characteristic of the dimensions of the probe. In general, at the jump, the magnitude of the change of force (per base atom) is larger and the probe–slab distance d_z smaller for probes of smaller cross-sectional area. These results are reproducible; repeated simulations for two arbitrarily chosen probes with different starting configurations revealed that the magnitude of the change in F_z, as well as the location of the jump d_z^{jump} was essentially the same. Apparently, as the probe is brought within a critical distance of the slab, forces between the two become sufficiently strong to overwhelm the bulk forces of the probe, which undergoes a significant deformation, signalled by the jump process.

To give further insight into the jump process, we present the results for the (6 × 6) probe as an example. Fig. 3 shows the

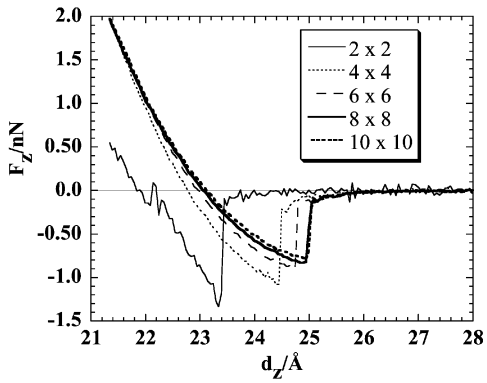

Fig. 2 Comparison of F_z profiles for all incoming probes.

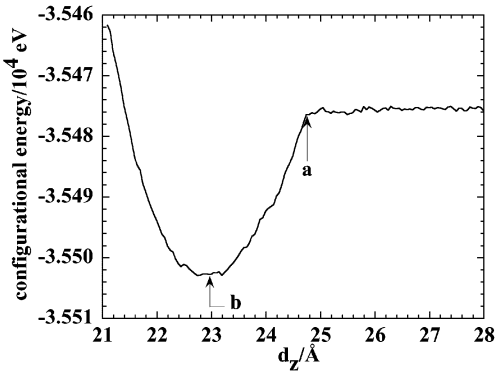

Fig. 3 Configurational energy profile of the (6 × 6) probe.

configuration energy profile for the (6 × 6) MgO probe. Point 'a' indicates the point at which the energy begins to change appreciably and also approximately marks the location of the steepest slope, where the attractive force would be at a maximum. This coincides with the onset of the jump seen in Fig. 2. Note that there is no substantial change in the energy for $d_z >$ a, an observation consistent with the small increase in attractive force seen Fig. 2. After the jump, the force becomes progressively more positive with decreasing d_z.

The structural changes that underlie the jump phenomenon are of particular interest. Fig. 4(a) and (b) show how the interplanar spacings of the probe and surface, respectively, change with the distance d_z. The spacings were of different values prior to the jump. It is well known that (001) MgO has only small surface relaxation, which does not significantly influence atoms beyond the first layer.[32] As a result, S2 and S3 are of similar value and slightly larger than S1 [Fig. 4(b)]. On the other hand, the non-periodic probe cluster [Fig. 4(a)] is slightly contracted and all the first three spacings are of smaller values to those of the slab. Unlike the slab, the effect of contraction is more pronounced deeper in the probe. As the probe

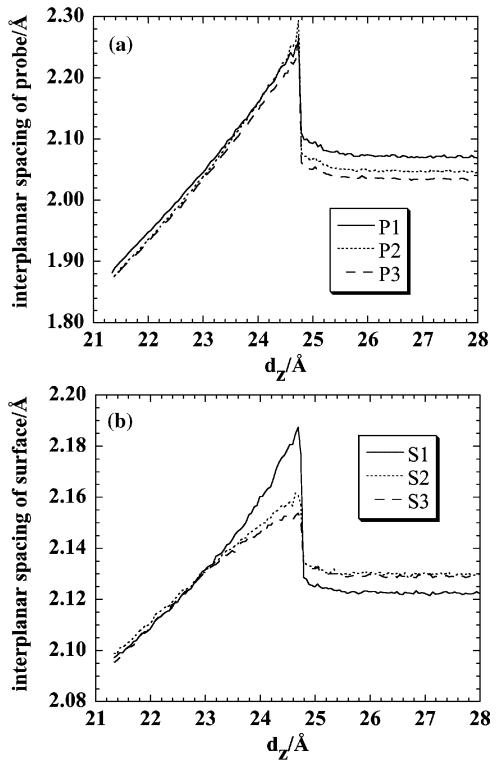

Fig. 4 Interplanar spacings profile for (a) the (6 × 6) MgO probe as it moves towards the surface and (b) the surface with the incoming (6 × 6) MgO probe.

moves towards the slab, both show a gradual increase in interlayer spacing. At the onset of the jump, atoms from as deep as the fourth layer beneath the surface are affected as all interlayer distances increase sharply. For the slab, the first layer jump is the most pronounced, with an increment of more than 0.06 Å. This is followed by the second and third spacings, which increase by about 0.03 and 0.02 Å, respectively. The subsurface slab displacements are less pronounced than for the probe, where the lower layers are less strongly anchored by bulk forces. Interestingly, all three observed spacings in the probe are rather similar after the jump, though significantly different before. This implies that the tension force is evenly distributed along the probe after the jump.

Fig. 5(a) shows the atomic configuration for the (6 × 6) probe at the jump region with the minimum F_z value. Note that the effects of attraction are apparent in atoms as deep as four layers beneath the surface. From visual inspection of Fig. 5(a)–(c), it is evident that the probe undergoes significantly more deformation than the slab. Note that lines are drawn between Mg and O atoms if the distance is around or less than the equilibrium value. Hence, some of the Mg–O bonds are not shown due to the Mg–O distances being larger than the equilibrium value. Similarly, diagonal lines are drawn when an Mg–O diagonal pair distance is closer than usual. This drawing convention is used for all atomic configurational figures and can be used as a rough guide to visualise the extent of the expansion or compression of a system.

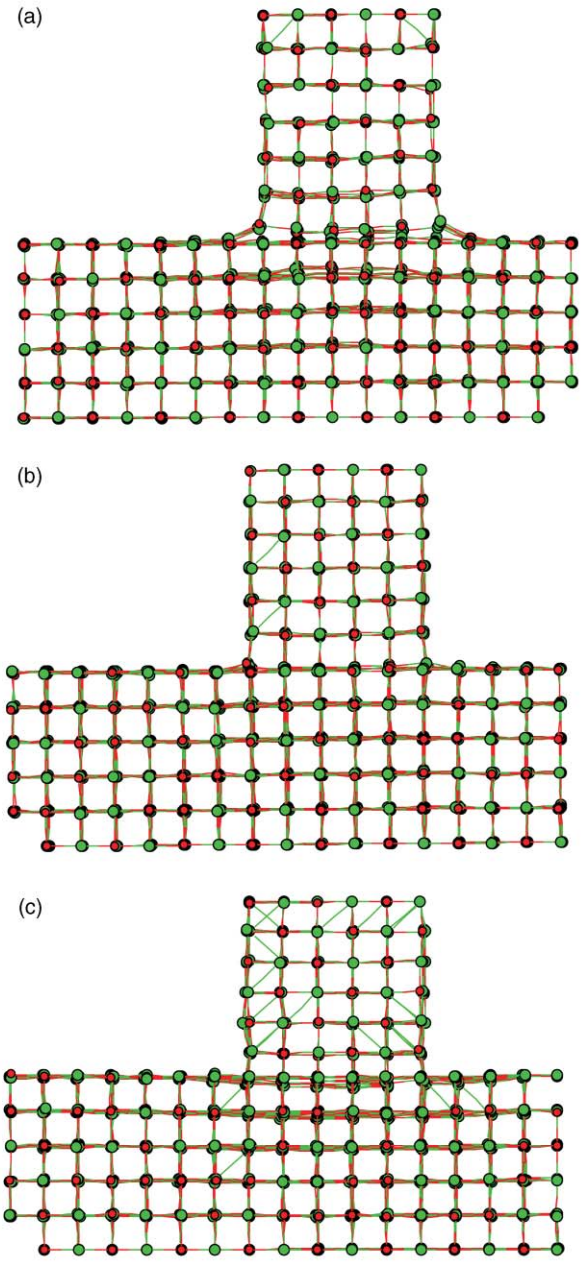

Fig. 5 Atomic configuration of (6 × 6) MgO probe: (a) minimum at d_z = 24.47 Å, F_z = −0.904 nN; (b) most stable atomic configuration at d_z = 22.97 Å and $F_z \approx 0.0$ nN; (c) most compressed state at d_z = 21.34 Å and F_z = +1.97 nN.

(iii) The approach to zero force. As the probe moves closer to the slab after the jump, F_z increases. The systems are not in compression at this stage, since the jump process results in the extension of both probe and slab, and the force remains negative until this extension is compensated for. This adjustment is shown in Fig. 2 as curvature of the plots after the jump process.

In Fig. 3, the minimum point (labelled b) of the configurational energy plot refers to the zero F_z value, *i.e.* where the system is energetically stable. As an example, for a (6 × 6) probe, d_z = 22.97 Å when $F_z \approx 0.0$ nN. This is the point at which all three observed interplanar spacings of the probe have values of ∼2.03 Å, which coincide rather closely with P2 and P3 prior to the jump, Fig. 4(a). Similarly, in Fig. 4(b), it can be seen that the three interplanar spacings of the slab merge at a value of ∼2.13 Å which is close to the inner second and third spacings (S2 and S3) prior to the jump. Fig. 5(b) shows the corresponding atomic configuration. At this stage, the probe is attached to the surface and is contiguous with the MgO bulk. Note, however, that the interplanar spacings of the probe are still slightly contracted in comparison with those of the surface.

(iv) Repulsion region. Beyond the jump region the force gradually increases and becomes positive as the probe begins to compress against the slab. Note that, with the exception of the (2 × 2) probe, all probes give slight curvature at the point of zero F_z. This shows that compression and extension at the equilibrium position are not Hookian in nature. There is, however, some linearity at the most highly compressed stage ($F_z > +1.0$ nN) where the F_z curves of various probes begin to merge.

Beyond the minimum energy configuration, the system is in compression. Fig. 5(c) shows the most compressed state obtained for the (6 × 6) probe, at d_z = 21.34 Å and F_z = +1.97 nN. The highly compressed state causes the body of the probe to thicken in the direction parallel to the surface plane, and the depression of the first and second surface layers is clearly seen.

Probe withdrawal from the surface

Overview of F_z profiles. The withdrawal of the probe from the slab followed a similar procedure to that which brought it down to the slab initially, *i.e.* incrementally at the same effective rate. This procedure gives rise to a series of complicated F_z plots, depending on the history of the system. In general, if the probe is withdrawn before the jump observed in the experiments above, the process of withdrawal is the simple reverse of bringing the probe towards the slab. In these cases, the F_z *versus* d_z plots are identical to those for the incoming probe. However, the F_z plots for withdrawal can be very different if obtained after a jump process has occurred. In these cases, the F_z profile departs from the incoming profile close to the location of maximum attractive force, such that F_z becomes larger than for the incoming case. Thereafter, the plots show a characteristic 'saw-tooth' pattern, indicating hysteresis, which we associate with structural changes in both the probe

and the slab, as is demonstrated below. We note also that the observed hysteresis becomes smaller as the probe size is increased and that separating the probe prior to the jump results in no hysteresis.

Thus, the withdrawal of the probe may be described by two distinct behaviours: (i) reversible, if withdrawal occurs when $d_z > d_z^{\text{jump}}$, and (ii) irreversible otherwise, the irreversible stage being characterised by a saw-tooth F_z profile indicating hysteresis in the withdrawal process.

Fig. 6(a) and (b) show the F_z profiles for the (2 × 2) probe and the (10 × 10) probe, respectively. In the former case, the smallest probe was withdrawn at the point where the jump had occurred, while the larger probe was withdrawn from the most compressed state. Each plot gives a very different F_z profile during the withdrawal. However, the saw-tooth pattern is evident in both. Each saw-tooth is comprised of a region with small negative slope followed by a large positive slope that rises over a narrow region of d_z. Visually, it resembles the jump seen in the advancing probe experiments. The region of negative slope indicates an increase in attractive force as the probe is withdrawn. It is noteworthy that this force may exceed the maximum observed after the jump in the previous experiments. This force is sufficiently strong to induce structural changes in the probe, which are signalled by the occurrence of the large positive slope of the saw-tooth. The saw-tooth pattern in Fig. 6(a) is more evident than in Fig. 6(b) because the structural changes of the smaller (2 × 2) probe represent a larger fraction of the bulk structure than in the larger (10 × 10) probe. These cases are described in greater detail below.

(i) The (2 × 2) probe withdrawal. We have found that for probes of all sizes, 'necking' processes are observed, whereby the cross-sectional area of probes and the contact area with surfaces decrease as probes are lifted. Fig. 7(a)–(d) show the atomic configurations of the (2 × 2) MgO probe at various distances. Their respective F_z values are indicated in Fig. 6(a). In general, Fig. 7 shows a succession of bonds breaking between atoms of adjacent planes and the formation of additional layers as the probe is lifted. This process is reflected in the saw-tooth pattern as shown in Fig. 6(a). Fig. 7(a) and (b) show a typical bond breaking process. In the former, the Mg–O bond which marked with an asterisk is highly stretched. As the probe is further lifted by 0.05 Å, the bond abruptly breaks, Fig. 7(b). The O atom from the probe subsequently forms an additional layer while the surface Mg atom re-embeds into the surface. The bond breakage also results in the top portion of the probe puckering. The process subsequently registers as a dip in F_z, as shown in Fig. 6(a).

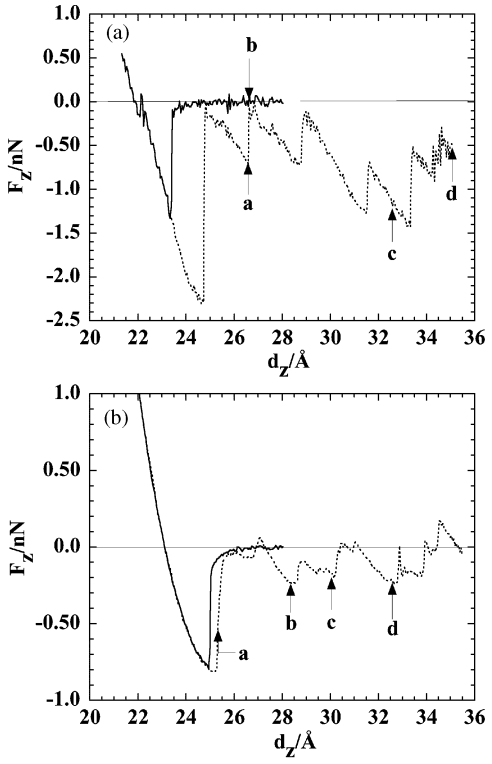

Fig. 6 Comparison of F_z profiles of incoming and withdrawing probes. The solid lines refer to probes moving towards the surface, and the dotted lines to those moving away. (a) The (2 × 2) MgO probe. The probe was withdrawn from the point where the first jump process occurred. Points 'a' to 'd' mark the corresponding atomic configurations as shown in Fig. 7(a)–(d). (b) The (10 × 10) MgO probe. The probe was withdrawn from the most compressed state. Points 'a' to 'd' mark the atomic configurations shown in Fig. 8(a)–(d).

As the probe is lifted further [Fig. 7(c)], complete narrowing of probe occurs. At this stage, the corresponding force measurement in Fig. 6(a) still shows increasing F_z in the negative direction (at the down slope of the saw-tooth pattern). This is due to the pulling of a surface atom pair towards the probe. The next dip in F_z refers to the breaking of bonds between these atoms and the surrounding slab. The extracted surface atoms attach to the probe and also to the adjacent pair of surface atoms. The whole process is repeated, whereby further separation of the probe results in the removal of the latter pair of surface atoms. Fig. 7(d) shows this effect at $d_z = 35.09$ Å. Here, two sets of MgO pairs have been completely separated from the surface with the creation of a hole defect in the slab surface.

(ii) The (10 × 10) probe withdrawal. Fig. 8 shows a sequence of atomic configurations as the (10 × 10) probe was pulled out. The corresponding values of F_z for the configurations are labelled in Fig. 8. Fig. 8(a) shows the initial formation of defects within the probe as the first few bonds break. The configuration corresponds to the region of steep change in F_z, as shown in Fig. 6(b). This dip is the most severe as it involves concurrent breakage of a series of bonds. The figure also indicates the source of the necking effect, where the initial narrowing effect of the probe is due to breakage of bonds within the body of the probe. The subsequent creation of the defect hole results in strain on atoms (marked with asterisks) that are near to the probe base and surface where some of the bonds have already broken. As the probe is withdrawn further from the surface, the defect hole enlarges and elongates, as shown in Fig. 8(b). The figure also shows the formation of the neck as the cross-sectional area is reduced from 10 to 8 columns while two additional layers are formed along the direction of the probe's movement.

The growth of the defect hole and subsequent neck narrowing can be seen in Fig. 8(b) and (c). Initially, the strain in the system steadily builds up until $d_z = 28.34$ Å, Fig. 8(b). At this stage the growth of the hole is initiated by the breakage of bonds of the atoms [marked as '+' in Fig. 8(b)] at the corner edge of the hole and propagated upward towards the surface edge of the probe. These atoms subsequently form part of the walls of the defect hole, as shown in Fig. 8(c). A narrowing effect occurs where atoms marked '#' are displaced towards the small gaps formed during the displacement of the '+' atoms. The numbering of layers in Fig. 8(b) and (c) is used to indicate the positions of the crystal layers.

Similarly, strain built up at the contact region causes bonds to break, as mentioned above. An elongated hole is subsequently produced, Fig. 8(d). At this stage the cross-sectional area is further reduced from 8 to 6 columns while two additional layers, one at the top and the other at the bottom of the hole, are produced along the direction of the probe's movement. This process is repeated, each time with a successive reduction of columns. We have terminated our simulations where the probe has been reduced to 4 columns. We believe

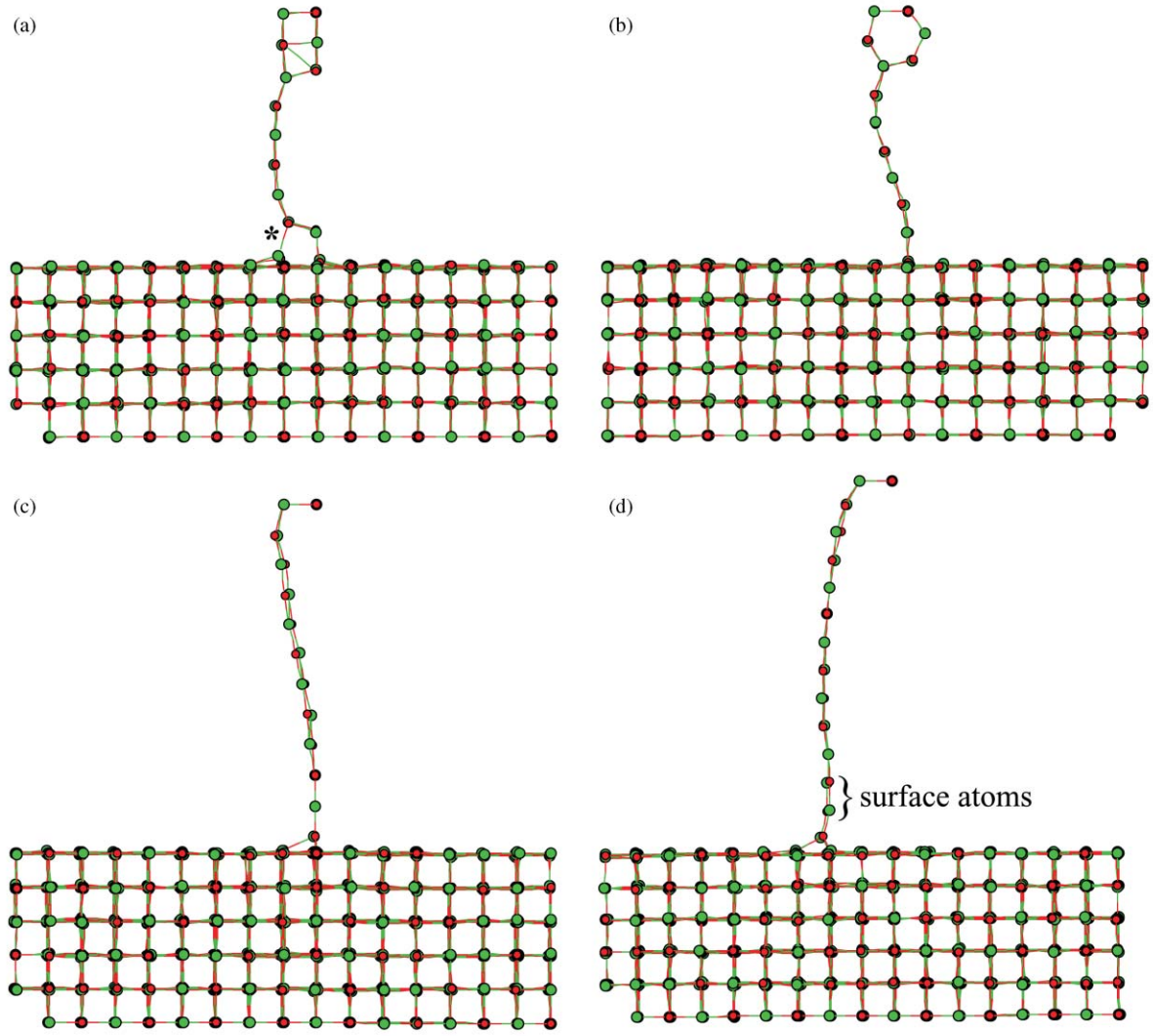

Fig. 7 Atomic configurations of (2 × 2) probe separation. (a) d_z = 26.59 Å; (b) d_z = 26.64 Å; (c) d_z = 32.59 Å; (d) d_z = 35.09 Å.

that further increasing d_z would eventually produce a single column string, as in the case of the (2 × 2) probe.

Finally, Fig. 9 shows how the interplanar spacings at the slab respond to the separation of the (10 × 10) probe. Note that at the initial jump location, hysteresis is observed as the probe is lifted. Much larger distance spacings result, which drop sharply at a large value of d_z, in marked contrast to the behaviour seen in the approach experiments. It can be seen that the saw-tooth curves correspond very closely with the F_z plot in Fig. 6(b). The first layer spacing is clearly more sensitive to the probe withdrawal process, while the effects on the subsequent spacings are similar in magnitude.

Similar processes are also found with probes of other sizes. However, no distinctive hole can be observed for smaller probes. Instead, gaps were produced with concurrent narrowing effects, which propagate along the probe. Similar neck structures were observed in most cases. Note that the narrowing effects and the subsequent neck formations mentioned above are one-dimensional in nature. This is even true for probes as small as (4 × 4).

Discussion

Our results show that the jump process is a characteristic feature of the MgO contact mechanism. Such features have been observed in other studies on both metal and metal oxide materials. In these studies, tip-shaped probes were used to study tip–surface contact[24,33,34] and tip–surface sliding.[26,34] However, in tip–surface contact studies, the force profiles usually show complex force variations at close surface distances after jump processes have occurred. This is due to the adsorption of additional surface ions to other parts of a tip as it is moving further into the surface.[34] In our case, no such adsorption has taken place and the curves show monotonous increases in F_z as the MgO blocks were compressed against the surface.

In our work, we found that the magnitude of the instability jump decreases as the size of the probe is increased. Fig. 10 shows a logarithmic plot of $|F_z|$ *versus* the cross-sectional area, A, of the probes. It reveals that the jump phenomena can be characterised by the simple relationship $|F_z| = kA^q$ with the contact exponent $q = -0.12$. In a subsequent study, we have repeated our calculations with NaCl, using potential parameters for NaCl obtained from Catlow *et al.*[35] The results are compared with the MgO in Fig. 10. The corresponding value of q for NaCl is -0.15 ± 0.01 which is fairly close to that for MgO. This suggests that the contact behaviour between any two crystalline solids with rock salt structures is rather similar. However, at this stage, we cannot claim that q is a universal quantity or even independent of the material structure, either crystalline or non-crystalline. The interatomic interactions in MgO are much stronger than those in NaCl. Therefore, it is apparent that q does not depend greatly on their magnitude.

From Fig. 2, we have also noted that the jump processes occur at larger values of d_z as the cross-sectional area of probes

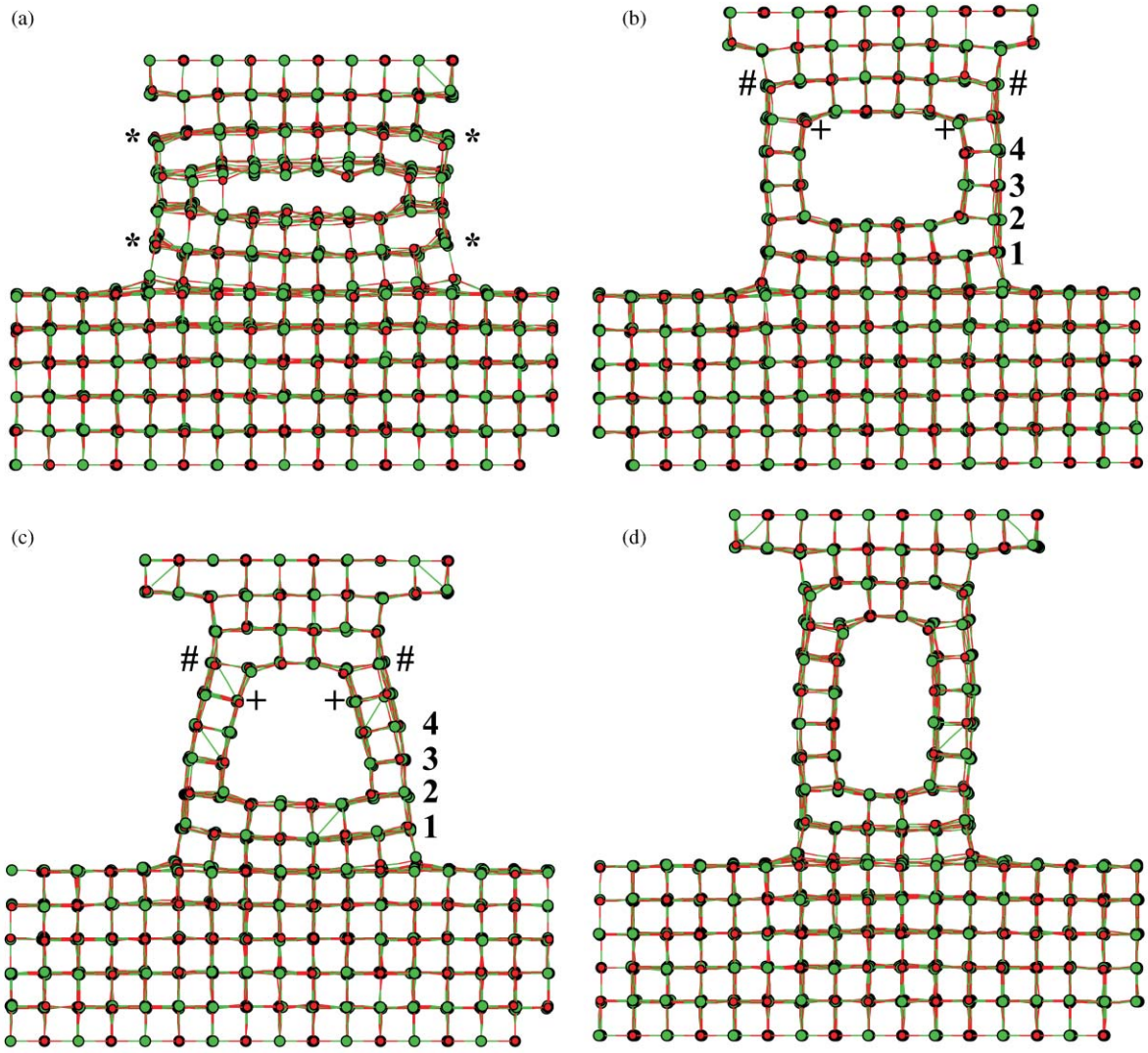

Fig. 8 Atomic configurations of (10 × 10) probe separation. (a) d_z = 25.34 Å; (b) d_z = 28.34 Å; (c) d_z = 30.04 Å; (d) d_z = 32.59 Å.

is increased. The origin of this behaviour is apparent in Fig. 11, which plots the relationship between the length of the isolated probes and d_z^{jump}, the vertical distance at which the jumps occur. A straight line has been drawn as a guide. Except for the smallest probe, a linear relationship is apparent. This indicates that it is the natural length of the probes, rather than the interatomic forces, that determine d_z^{jump}. The narrower isolated probes are more contracted and, as a result, must approach closer to the surface for the jump to occur. It is also apparent that larger probes behave increasingly similarly to the slab and hence the differences in d_z^{jump} become smaller. In fact, results from Fig. 1 show that the largest (10 × 10) probe has a value of d_z^{jump} only marginally larger than that of the (8 × 8) probe, suggesting that largest probe is reaching the limiting behaviour as a slab. This is also confirmed from the interlayer spacing measurements. For example, the value of P1 for the

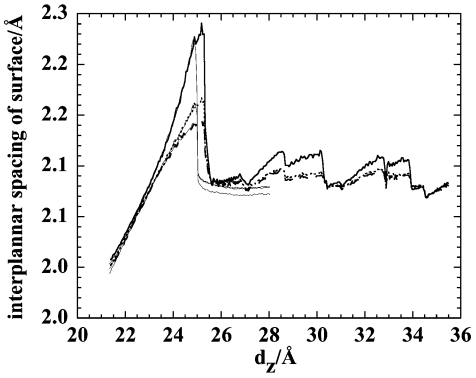

Fig. 9 Interplanar spacing profile for (10 × 10) MgO probe. Solid lines refer to the first three interplanar spacings as the probe approaches the surface. They are qualitatively similar to Fig. 4(b). The bold lines refer to the interplanar spacings when the probe is withdrawn. Bold solid line, S1; bold dotted line, S2; bold long dash line, S3. S2 and S3 are practically merged after the first large drop (see text).

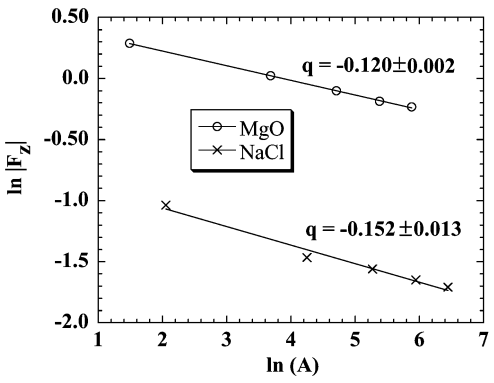

Fig. 10 Logarithmic plot of $|F_z|$ *versus* area of the rigid plane in probes.

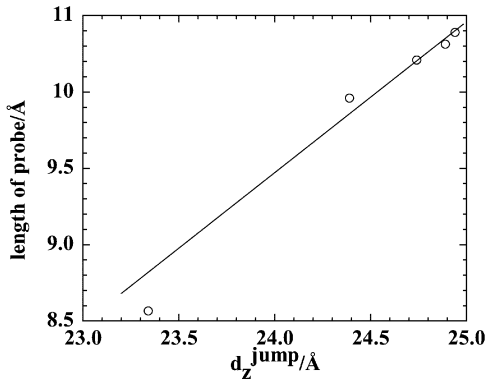

Fig. 11 Length of probes (between base and active surface) *versus* vertical distance, d_z^{jump}, at which the 'jumps' occur.

largest probe is about 2.1 Å, whereas it is about 2.12 Å for the slab.

According to the theory of friction,[36] and experimentally,[37] the area of contact is proportional to load. In Fig. 12 we have plotted the total load at d_z^{jump} *versus* the area of the probe at contact. The result shows the contact load is indeed proportional to contact area. This suggests that the jump process may be a fundamental component of friction. Theory assumes that frictional contact is mediated by surface roughness. In our case, it is interesting to note that the probe consists of a plane that is atomically smooth apart from surface rumpling and thermal fluctuation. The contact between the slab and the probe can be regarded as 'point-to-surface' mode, albeit that the 'point' in this case refers to an atomically smooth plane of finite area.

As the probes are withdrawn from the slab, the resulting hysteresis is independent of the extent of probe penetration. Prior to the jump process, probe penetration is perfectly reversible and there is no noticeable disruption to the slab structure. This is in contrast with the experimental work using much softer materials such as surfactant monolayers.[38] In this case, the observed hysteresis is believed to be due to the extent of interpenetration and ease of disentanglement of the molecules across the junction. These conditions, in turn, depend on the structural phase at the junction. For example, frictional forces and the hysteresis increase as the surfactant molecules become more amorphous due to increase in chain entanglement. In contrast, both friction and hysteresis are small when the molecules are solid-like with little interpenetration.

From the point of view of friction, the hysteresis observed when the probes are withdrawn is a means by which energy is dissipated in the system and thus a significant contributor to friction.

In all cases seen here (as in other studies), a necking process is observed. This involves plastic flow with systematic atomic dislocation as the probes are drawn away from surface. During the separation process, the system response is essentially elastic (at the slope of the saw-tooth F_z curve) until a yield point is reached, where stored energy is suddenly released by bond breakage accompanied by layer additions. This causes a dip in the F_z measurements. In previous work by others concerning Ni tip indentation of Au surfaces and *vice versa*,[24] similar necking and elastic response is also reported. In this case, the necking involves elongation of the softer Au material. However, complete separation of the Ni tip is possible where some Au atoms were attached to various positions on the surface of the tip, with some vacancies and substitutional defects on the substrate surface. In addition, a similar observation is also reported from the other work involving retraction of an MgOH tip from an NaCl surface.[34] However, our studies show rather different 'wetting' behaviour for MgO. In this case, a defect hole is created and enlarged when pairs of surface Mg–O atoms are systematically stripped away and attached to the ends of the probes. This would only occur after complete narrowing of the probe has been achieved. It is not clear if the separation process is dependent on the shape of the probe. In other studies, a tip-like structure is usually used, whereas in our case the probe is a rectangular block where penetration of the probe into the surface may be less effective and involve different mechanisms.

Finally, we note that we have used a simple rigid ion model in our calculations. We believe that using a more sophisticated model, such as the shell model,[39] for polarisability would yield similar qualitative results. For a study of the general contact behaviour of the material, exact quantitative comparison is not essential.

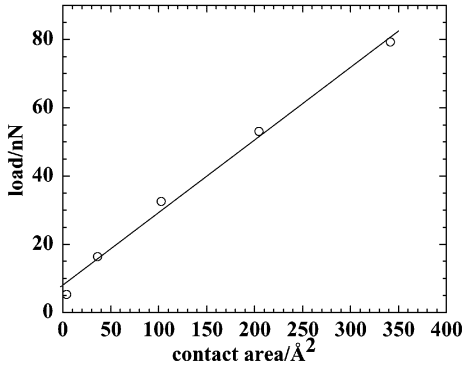

Fig. 12 Load at the base of probes at d_z^{jump} *versus* contact area.

Summary

We have employed molecular dynamics computer simulations to study in detail the contact behaviour of MgO crystalline samples. Several important phenomena have been observed, particularly the occurrence of a 'jump' process when a probe sample nears a surface, and the hysteresis in the withdrawal of the probe after the jump has occurred. The jump process was described by a simple empirical relation between the cross-sectional area of the probe and the measured attractive force at the time of the jump. The relevance of these contact processes to the origin of friction has been discussed. Several issues need further clarification. For example, the characteristics of the q exponent and whether it can be described on other more complicated crystalline structures such as TiO_2. Furthermore, a previous study[38] concluded that the frictional force is not related to the adhesion force, but rather to the hysteresis associated with the adhesion force. It would therefore be interesting to measure frictional force at different values of d_z and to determine the associated atomic mechanisms involved between two sliding MgO bodies. These studies will be published in subsequent papers.

Acknowledgement

This research was carried out under a research grant from the EPSRC. The simulations were performed on the Daresbury Laboratory IBM SP/2 computer. We are grateful to L. V. Woodcock for helpful discussions.

References

1 C. S. Campbell, *Annu. Rev. Fluid Mech.*, 1990, **22**, 57.
2 L. P. Kadanoff, *Rev. Mod. Phys.*, 1999, **71**, 435.
3 P. A. Cundall and O. D. L. Strack, *Geotechnique*, 1979, **29**, 47.
4 D. Hirshfeld and D. C. Rapaport, *Phys. Rev. E*, 1997, **56**, 2012.
5 J. Baxter, U. Tüzün and J. Burnell, *Phys. Rev. E*, 1997, **55**, 3546.
6 S. McNamara and W. R. Young, *Phys. Rev. E*, 1996, **53**, 5089.

7 P. A. Langston, U. Tüzün and D. M. Heyes, *Powder Technol.*, 1995, **85**, 153.
8 P. A. Langston, U. Tüzün and D. M. Heyes, *Chem. Eng. Sci.*, 1995, **50**, 967.
9 T. Pöschel and V. Buchholtz, *Phys. Rev. Lett.*, 1993, **71**, 3963.
10 *Fundamentals of Friction: Macroscopic and Microscopic Processes*, ed. I. L. Singer and H. M. Pollock, Kluwer, Dordrecht, 1992.
11 E. Rabinowicz, *Friction and Wear of Materials*, Wiley, New York, 1965.
12 G. M. McClelland and J. N. Glosli, in *Fundamentals of Friction: Macroscopic and Microscopic Processes*, ed. I. L. Singer and H. M. Pollock, Kluwer, Dordrecht, 1992, 405.
13 F. P. Bowden and D. Tabor, *Friction and Lubrication of Solids*, Clarendon, Oxford, vol. 2, 1964.
14 G. Binnig, C. F. Quate and Ch. Gerber, *Phys. Rev. Lett.*, 1986, **56**, 930.
15 C. M. Mate, G. M. McClelland, R. Erlandsson and S. Chiang, *Phys. Rev. Lett.*, 1987, **59**, 1942.
16 O. Marti, J. Colchero and J. Mlynek, *Nanotechnology*, 1990, **1**, 141.
17 M. Hirano and K. Shinjo, *Phys. Rev. B*, 1990, **41**, 11837.
18 J. B. Sokoloff, *Phys. Rev. B*, 1990, **42**, 760.
19 B. N. J. Persson, *Phys. Rev. Lett.*, 1993, **71**, 1212.
20 P. A. Thompson and M. O. Robbins, *Phys. Rev. A*, 1990, **41**, 6830.
21 B. N. J. Persson, *J. Chem. Phys.*, 2000, **113**, 5477.
22 J. A. Harrison, C. T. White, R. J. Colton and D. W. Brenner, *Phys. Rev. B*, 1992, **46**, 9700.
23 K. J. Tupper and D. W. Brenner, *Thin Solid Films*, 1994, **253**, 185.
24 U. Landman, W. D. Luedtke and E. M. Ringer, in *Fundamentals of Friction: Macroscopic and Microscopic Processes*, ed. I. L. Singer and H. M. Pollock, Kluwer, Dordrecht, 1992, 463, and references therein.
25 D. W. Brenner and J. A. Harrison, *Am. Ceram. Soc. Bull.*, 1992, **71**, 1821.
26 A. L. Shluger, R. T. Williams and A. L. Rohl, *Surf. Sci.*, 1995, **343**, 273.
27 J. A. Harrison, D. W. Brenner, C. T. White and R. J. Colton, *Thin Solids Films*, 1991, **206**, 213.
28 W. Smith and T. R. Forester, DL_POLY, version 2.12, CCLRC, Daresbury Laboratory, Warrington, UK.
29 H. J. C. Berendsen, J. P. M. Postma, W. F. van Gunsteren, A. DiNola and J. R. Haak, *J. Chem. Phys.*, 1981, **81**, 3684.
30 C. R. A. Catlow, I. D. Faux and M. J. Norgett, *J. Phys. C*, 1976, **9**, 419.
31 A. R. Leach, *Molecular Modelling: Principles and Applications*, Longman, Singapore, 1996.
32 E. A. Colbourn, J. Kendrick and W. C. Mackrodt, *Surf. Sci.*, 1983, **126**, 350.
33 A. L. Shluger, A. L. Rohl, D. H. Gay and R. T. Williams, *J. Phys. C*, 1994, **6**, 1825.
34 A. L. Shluger, A. L. Rohl, R. T. Williams and R. M. Wilson, *Phys. Rev. B*, 1995, **52**, 11398.
35 C. R. A. Catlow, K. M. Diller and M. J. Norgett, *J. Phys. C*, 1977, **10**, 1395.
36 J. A. Greenwood, *Trans. ASME*, 1967, **89**, 81.
37 C. M. Mate, G. M. McClelland, R. Erlandsson and S. Chiang, *Phys. Rev. Lett.*, 1987, **59**, 1942.
38 H. Yoshizawa, Y-L. Chen and J. Israelachvili, *J. Phys. Chem.*, 1993, **97**, 4128.
39 B. G. Dick and A. W. Overhauser, *Phys. Rev.*, 1958, **112**, 90.